ELSEVIER

Cement & Concrete Composites 23 (2001) 299–311

Cement & Concrete Composites

www.elsevier.com/locate/cemconcomp

Gypsum morphological analysis and modeling

D. Jeulin [a,*], P. Monnaie [b], F. Péronnet [c]

[a] Centre de Morphologie Mathématique, ENSMP, 35, rue Saint-Honoré, F77300 Fontainebleau, France
[b] Previously in LMS, Ecole Polytechnique, F91128 Palaiseau, France
[c] Lafarge LCR, 95, rue de Montmurier, B.P. 15, F38291 Saint Quentin-Fallavier Cedex, France

Abstract

When plaster is put in water, a network of needles is spontaneously formed. The morphology of the plaster microstructure have been studied in order to understand precisely its role with respect to its physical properties. Three microstructures of plaster were prepared from different hydration conditions, to obtain three crystal sizes at a given level of porosity. We propose a morphological characterization and modeling of the plaster microstructure by means of simple tools of mathematical morphology. From the use of a two parameters random model of microstructure, the Boolean model, contact properties between the microstructural units made of gypsum needles are estimated, and bounds of the elastic behavior of the plaster are compared to measurements.

Keywords: Plaster; Porous media; Image analysis; SEM; Surface of contact; Boolean model; Young's modulus; Bounds

1. Introduction

The microstructure of plaster, made of needle shaped gypsum crystals, changes with many parameters such as the hydration conditions, the properties of gypsum and of additives used in its preparation.

It is important to study the morphology of plaster microstructure, to understand better its influence on such properties as cracking mechanisms, and elastic properties.

In this paper, some aspects of plaster porous microstructure are recalled, from samples examined in the scanning electron microscope (SEM). Then are introduced the main morphological parameters used to characterize this microstructure. The arrangement of crystals can be described by a model of random medium, the Boolean model, with parallelepiped grains, which can reproduce the morphological arrangement of some plasters. Finally, estimations of the elastic moduli of plasters obtained from the Boolean model are compared to measurements.

2. Plaster porous microstructure

The morphology of gypsum crystals in plaster is a result of the conditions of the hydration reaction. By changing the parameters of each step (dissolution, nucleation, growth), various plaster microstructures are obtained. They are made of elongated and interlocked crystals, which give the stiffness of the material. The variations of hydration conditions change the degree of interlocking, the texture, and the size distribution of crystals.

In the present study, the samples were prepared by varying the temperature of hydration or the amount of crystallization seeds according to [1]. The samples will be named "reference" (20°C), "gypseous" (gypsum seed addition), and 70°C.

From SEM micrographs of fracture surfaces, an estimation of crystals sizes, assimilated to parallelepiped rods (with sides l, L, e) was given [1]. The measurements were made by hand at a $\times 1000$ magnification, on crystals orthogonal to the electron beam. Submicronic crystals were not taken into account in this estimation. The lengths below are indicative, and are given in μm.

Sélecta prepared with 0.025% gypsum:	$L = 10$, $l = 1.25$, $e = 0.75$.
Sélecta prepared at room temperature:	$L = 25$, $l = 3$, $e = 1.75$.
Sélecta prepared at 70°C:	$L = 53.5$, $l = 9.5$, $e = 5.5$.

* Corresponding author. Tel.: +33-1-64692795; fax: +33-1-64694707.
E-mail address: jeulin@cmm.ensmp.fr (D. Jeulin).

0958-9465/01/$ - see front matter
PII: S0958-9465(00)00066-4

These measurements reflect the expected influence of parameters on the crystals size: the 70°C sample owns the larger crystals with the lower elongation ratio L/l. Crystals are much smaller and interconnected for the gypseous case. Some specific crystal arrangements similar to sea urchins (gypseous) or bundles (70°C) appear. This is illustrated by the SEM micrographs of Fig. 1.

A further approach of the microstructure can be made by means of image analysis. For this purpose, images were obtained in four steps: the preparation of plaster specimens, of polished sections, the acquisition of images in the SEM, and the processing of images to obtain binary images by thresholding.

Specimens were obtained with a controlled time of preparation of mixes and of the drying process (three days at 45°C). Polished sections are made from samples where pores are filled under vacuum by an epoxy resin [1]. One polished section was made for each material.

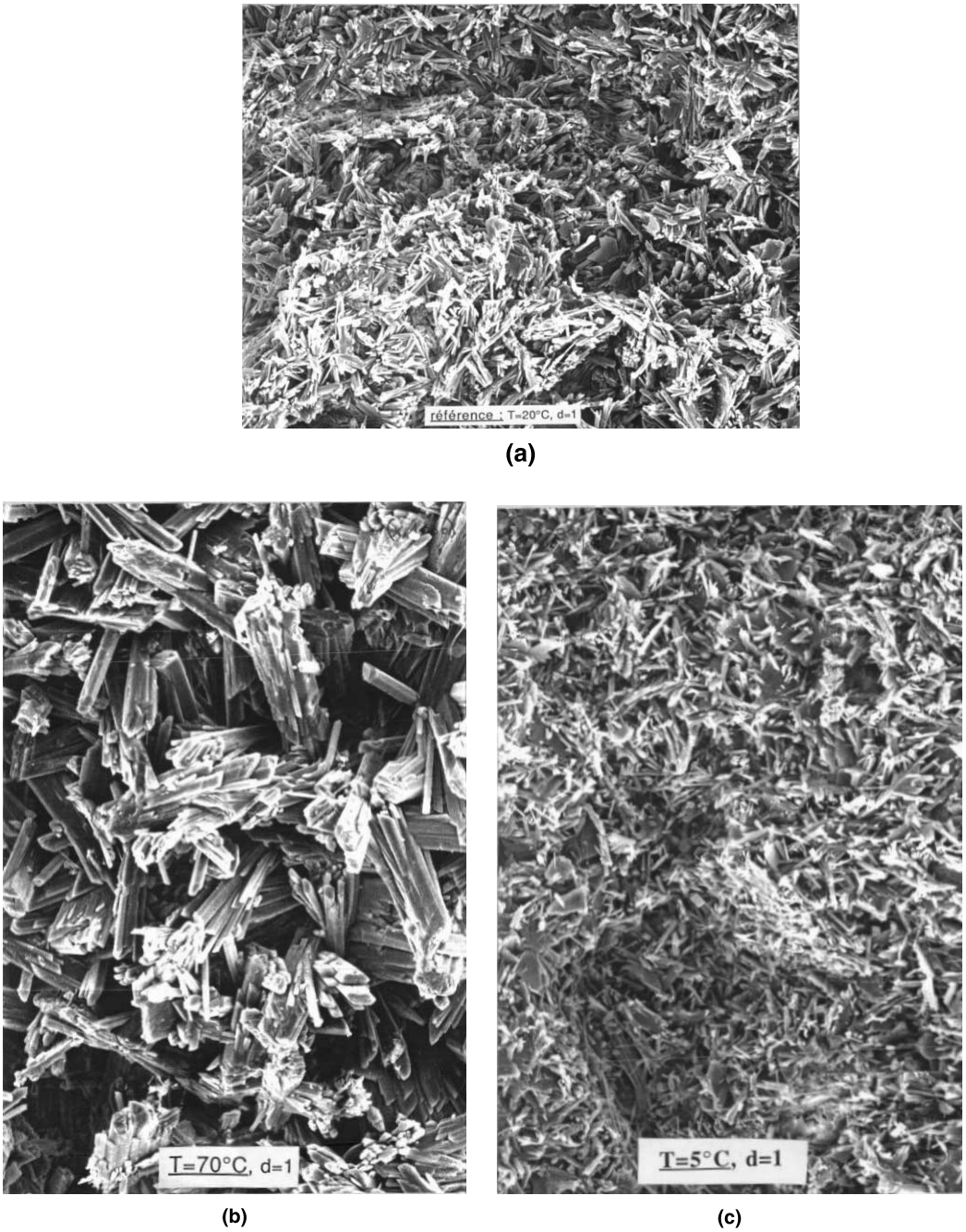

Fig. 1. SEM micrographs of the three studied plasters [1]: (a) reference; (b) prepared at 70°C; (c) gypseous. Magnification ×1000.

Table 1
Studied materials

Type of plaster	Gypseous	Reference	70°C
Medium magnification	550	200	100
High magnification	1000	500	250

Table 2
Scale of images at different magnifications

100 μm = 54 pixels	$G = 100$
100 μm = 112 pixels	$G = 200$
100 μm = 141 pixels	$G = 250$
10 μm = 26 pixels	$G = 500$
10 μm = 31 pixels	$G = 550$
10 μm = 56 pixels	$G = 1000$

After metallization, the sections are examined in a SEM, where the backscattered electrons mode is used for imaging: gypsum appears in white, and pores in black. Two magnifications (given in Table 1), were used for each specimen, in order to be able to compare the measurements obtained for the wide range of crystal sizes; 10 grey levels (8 bits) images (640×412 pixels) were obtained at a medium magnification, and twenty images for the higher (Table 1).

The scale of images is given in Table 2, the distance between two pixels depending on the magnification.

Grey level images were transformed into binary images by the choice of thresholds according to a "maximization of the average global contrast" using the method proposed in [2]. The result is illustrated in Fig. 2. To check the validity of the image acquisition process, one can compare the pore volume fraction V_V, estimated from image analysis and from the density d of samples ($V_V = d/2.32$, 2.32 being the density of gypsum), as shown in Table 3.

There is a good agreement, but sometimes the pore volume fraction obtained by density is out of the confidence interval (± two standard deviations divided by $\sqrt{n}$ for n images). This is due to the choice of the thresholds, which can induce variations of up to 5% for the volume fraction of gypsum.

3. Morphological characterization

In order to obtain a quantitative morphological description of plaster, a mathematical morphology [3] based approach was used. Morphological information is obtained in two steps: the transformation of the image, followed by measurements. A full description of the microstructure can be obtained by means of models of random media, such as the Boolean model.

3.1. Basic morphological measurements

The basic measurements are derived from integral geometry [3–5]. They satisfy strong experimental constraints, such as: the invariance by translation, continuity (with respect to the approximation of objects), the access over restricted fields of measurement, additivity (to be able to make averages), and good stereological properties (giving access to 3D information from 2D images). The basic measurements are detailed in Appendix A. For a random set A, the Minkowski functionals (Appendix A) become random variables. For a stationary random medium, such as a porous medium, the statistical properties are invariant by translation, and one can define specific properties per unit volume (S_V: specific surface area, V_V: volume fraction, etc.). These properties (with the exception of the 3D connectivity number N–G) can be estimated from lower dimensional measurements by means of stereological relationships.

3.2. Basic transformations of mathematical morphology

To describe a microstructure, one can compare it to usual reference shapes, namely to compact sets K with a given shape [3–5]. The basic morphological transformations are the operations of erosion and of dilation (defined by Eqs. (A.1)–(A.3) in Appendix B). By combining these two operations, it is possible to define two new operations, the opening (erosion followed by a dilatation) and the closing (dilation followed by an erosion). Using convex sets K, they give access to the estimation of size distributions of X and of X^c.

4. Model of random microstructure

To represent the morphology of textures as seen in the plaster microstructure, it is useful to use models of random sets, as proposed earlier for any two-phase medium [4–6].

4.1. Principle and application to gypsum microstructure

To completely characterize a random closed set A, we need to know its probabilistic properties through the laws $T(K)$ defined in Appendix C (Eq. (A.4)). These are a generalization of the well-known notion of probability distribution that is used to characterize a random variable. The probabilistic properties of a random set are used to test a model, to estimate its parameters, and to predict morphological properties which are not directly available from experiments. They are estimated from the measurement of volume fractions after dilations (Eq. (A.5)).

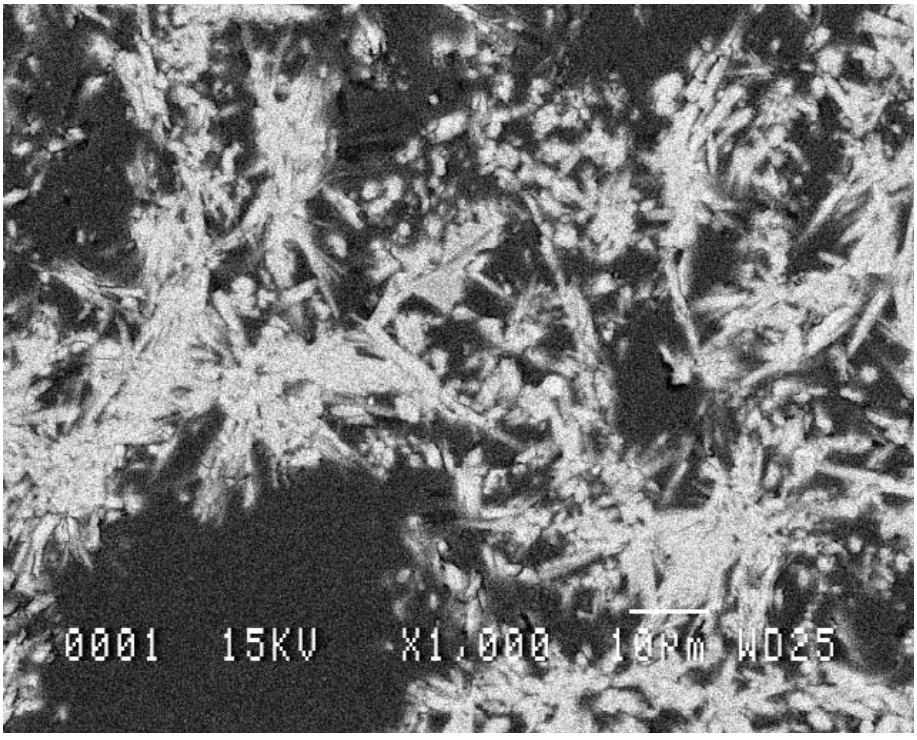

(a)

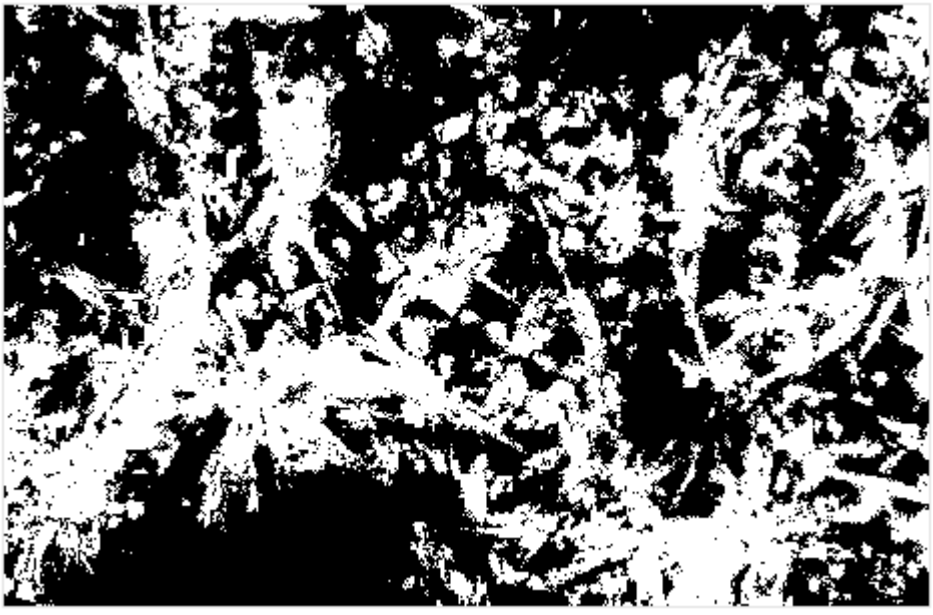

(b)

Fig. 2. Example of a SEM micrograph of a polished section (a), and resulting binary image obtained by thresholding (b) Reference plaster.

The covariance of pores $Q(h)$ (i.e., the probability for the two points $\{x, x+h\}$ to remain inside pores, given in Eq. (A.6)) and the function $Q(l)$, obtained for segments of length l, reflect anisotropy of the microstructure, since they depend on the orientation of the vector h or of the segment l. We tried to detect them by estimating $Q(h)$ and $Q(l)$ on two orthogonal directions (called horizontal and vertical) from 2D images. No significant anisotropy was detected from the measurements, as illustrated by one example on Fig. 3.

We can estimate for every structure its correlation length, defined as the length where $Q(h)$ reaches its

Table 3
Comparison of the gypsum fraction measured by density and by image analysis[a]

Reference	Gypseous (0°)		Reference (23°)		70°	
Magnification	550	1000	200	500	100	250
Gypsum fraction (density)	0.420		0.421		0.427	
Gypsum fraction (images)	0.399	0.394	0.410	0.419	0.462	0.430
Gypsum fraction (lower)	0.380	0.369	0.391	0.397	0.458	0.421
Gypsum fraction (upper)	0.417	0.420	0.429	0.441	0.467	0.440

[a] Upper and lower values correspond to the confidence interval resulting from statistical variations in images.

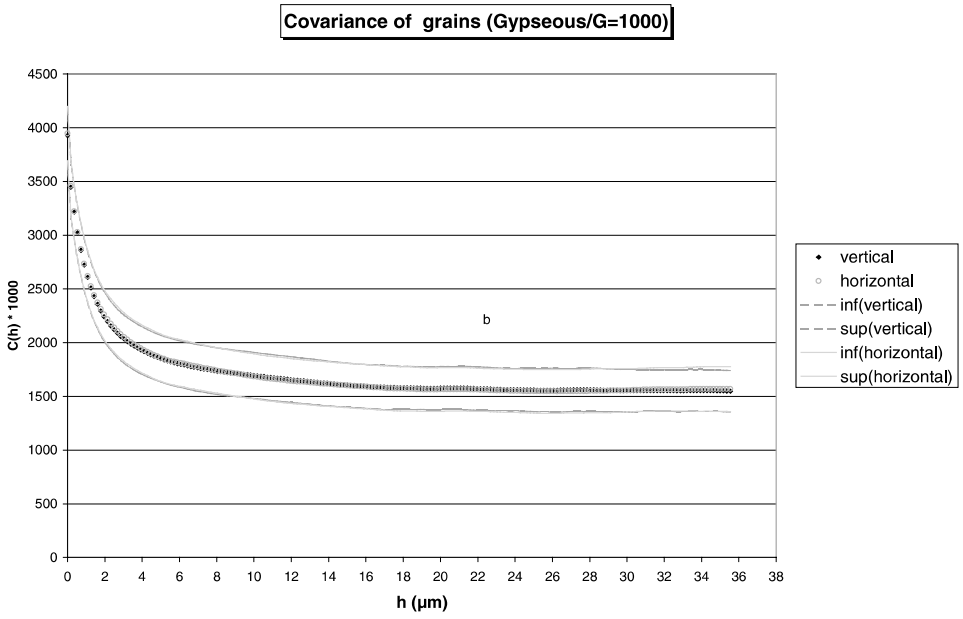

Fig. 3. Vertical and horizontal covariance with their intervals of confidence (gypseous plaster).

Table 4
Correlation lengths in μm

Reference	Gypseous (0°)		Reference (23°)		70°	
Magnification	550	1000	200	500	100	250
Correlation length[a] (grain)	12	12	24	25.5	22	20
Correlation length[a] (pore)	14	11.5	25	20.5	22	18
Correlation length[b] (grain)	29	23.5	41	65	36	123.5
Correlation length[b] (pore)	40	28.5	43	32	39	27

[a] Abscissa from which the reduced centered covariance is lower than 5%.
[b] Abscissa from which the reduced centered covariance is lower than 1%.

asymptotic value q^2. When this length is reached, the events $\{x$ belongs to pores$\}$ and $\{x+h$ belongs to pores$\}$ become statistically independent, which means that we get the size of a representative volume element of the microstructure. It should be the same for the two sets grains and pores, but slight differences are experimentally observed (Table 4), mainly because its experimental determination is not very accurate, due to the statistical fluctuations of the experimental curve $Q(h)$. It also depends on the magnification in some cases, due to the occurrence of scales superimposition. Since the correlation lengths remain lower than the size of the fields of measurement, we can consider that the used magnifications are correct with respect to the microstructure. The

covariance is used later for the estimation of parameters of models of random sets.

4.2. Boolean model

One could conclude a morphological study of the gypsum microstructure by the restricted data set of measurements obtained on images. However, some interesting parameters like the area of contact between crystals, the number of crystal germs per unit volume, the connectivity number in three dimensions, 3D size distributions of pores, would be useful to explain physical properties of gypsum. However, this information cannot be obtained from measurements on two-dimensional sections. In addition, it can be useful to summarize the complex morphology of gypsum by few parameters, and to provide means to generate simulations of three-dimensional images of this material. This can be a first step in the calculation of its overall properties, as will be introduced below. An approach based on the implementation of models of random sets will enable us to describe the morphology of gypsum in a synthetic way. The Boolean model [3–8] is one of the simplest models of two phase materials, which reproduces overlapping grains in space. It is therefore, a good candidate for gypsum microstructure. It is obtained in two steps:

- implantation of Poisson points x_k with the intensity (average number per unit volume) θ in the space,
- implantation of a random primary grain A' on every Poisson point, with possible overlaps between grains.

The material A is obtained by $A = \cup_{xk} A'_{xk}$. The main probabilistic properties of this model that are used in the present study, are given in Appendix D.

4.3. Results

4.3.1. Test of the model

Linear and hexagonal erosions are used to test the validity of the assumption of a Boolean model with convex grains (Appendix D). In this case, the logarithm of the experimental curves $Q(l)$ and $H(d)$ should be polynomials of degree 1 and 2. The linear behaviour of $\log(Q(l))$ is observed over several orders of magnitude (3–4), for pores (Fig. 4) as well as for grains. A small part is nonlinear over short distances ranging from 4 to 10 μm, depending on the material. This is due to irregularities of the boundary of gypsum grains on a small scale. From these simple tests, grains and pores can be candidates as convex primary grains of a Boolean model. Nevertheless, these primary grains will be affected to gypsum crystallites.

The next step will be the choice of the shape of grains. As seen before, the three studied microstructures are textures of gypsum needles with frequent hexagonal sections. More simple shapes will be used: Poisson polyhedra, parallelepipeds with a square basis and Poisson parallelepipeds. The parameters of the models are estimated by fitting the experimental curves of the reduced geometrical covariogram of grains $r(h)$ (deduced from the covariance $Q(h)$ by means of Eq. (A.10) for the intermediary magnification) to the theoretical ones.

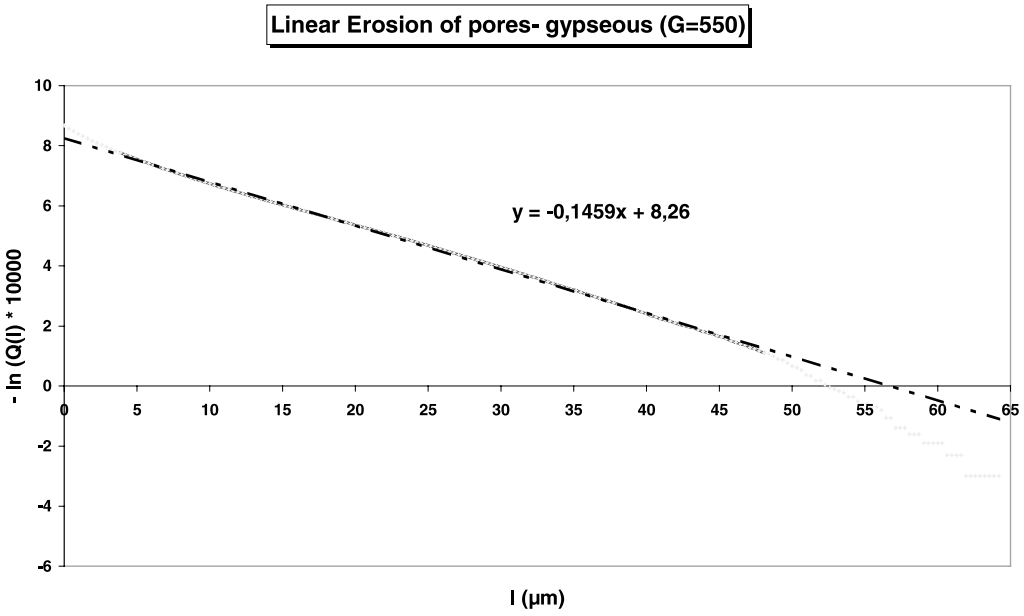

Fig. 4. Curve $\log(Q(l))$, $Q(l)$ being the probability for the segment l to be included in the pores of the material, for the gypsous plaster ($G = 550$). An exponential behaviour is observed, which is in agreement with a Boolean model with convex primary grains for simulating the texture of gypsum crystals.

4.3.2. Average size and surfaces of contact

From the slope of $Q(l)$, we can estimate the average chord length L, and the specific surface area S_v. For a Boolean model, we have:

$$S_V = -4Q'(0) = -4\theta q K'(0) = \theta q S(A'), \quad L = -Q'(0)/Q(0), \tag{1}$$

where $S(A')$ is the surface area of the primary grain A'. Note that $\theta S(A')$ is the slope of log $(Q(l))$.

One can consider contacts between grains from the two following points of view:

- The probability distribution of the number of primary grains covering a point x. The random number of grains A' covering x follows a Poisson distribution with expectation log $(q) = \theta V(A')$. This parameter, which does not depend on the shape of primary grains, is directly obtained from q.
- The contact surface area between primary grains. It can be estimated by the difference between the specific surface areas of a Boolean model with the same grains, but limited to their boundary (and therefore with a zero volume fraction, $q = 1$), and the specific surface area given by Eq. (1). The surface area of empty grains is given by $\theta V(A')$. Then, the specific surface area of bounds between grains is given by:

$$S_{Vc} = \theta(1-q)S(A').$$

One can also use the surface area per grain covering a point:

$$\frac{S_{Vc}}{(\theta V'(A')} = \frac{S(A')}{V(A')}(1-q) = \frac{Q'(0)}{\ln q}(1-q). \tag{2}$$

The slopes estimated on $Q(l)$ curves are stable with respect to magnification, which give a reliable measurement (Table 5). Using the slope at the origin provides us with a lower average L, due to the presence of some roughness of the grain boundaries. For the two estimations of L, the average sizes of grains and pores increase with the temperature, as a result of a coarser microstructure.

The various specific area are given in Table 6. They all decrease with the temperature, reflecting again the coarsening of the microstructure. The contact surface area and the toughness of plasters have not the same evolution; we should probably in addition account for the crystals orientations of grains in contact.

4.3.3. Poisson polyhedra

Poisson polyhedra [3–6] are obtained from Poisson flats, which are a Poisson point process on the space $S \times R^+$ (where S is the unit sphere in R^3 and R^+ the positive real numbers) with the intensity $\lambda(\mathrm{d}u)\mathrm{d}x$. These flats enclose Poisson polyhedra. For isotropic materials,

Table 5
Slopes of the curves $Q(l)$, and average chord length

Reference	Gypseous (0°)		Reference (23°)		70°	
Magnification	550	1000	200	500	100	250
Estimated slope (pore) (μm^{-1})	0.15	0.15	0.06	0.07	0.05	0.06
Estimated slope (grain) (μm^{-1})	0.23	0.28	0.1	0.1	0.07	0.08
Estimated length (pore) (μm)	4.12	4	9.77	8.7	10.3	10.03
Estimated length (grain) (μm)	1.74	1.43	4.09	4.18	6.77	5.29
Slope at the origin[a] (pore) (μm^{-1})	0.32	0.47	0.12	0.18	0.07	0.09
Slope at the origin[a] (grain) (μm^{-1})	0.49	0.73	0.18	0.26	0.08	0.11
Average length (pore) (μm)	1.86	1.29	4.76	3.15	8.13	6.7
Average length (grain) (μm)	0.82	0.54	2.23	1.62	5.94	3.79

[a] $\mathrm{d}(\ln[P(l)])/\mathrm{d}h(h=0)$.

Table 6
Specific surface areas

Plaster	Gypseous (0°)		Reference (23°)		70°	
Magnification	550	1000	200	500	100	250
Specific surface area (μm^{-1})	0.088	0.092	0.036	0.039	0.028	0.032
Specific surface area of bonds (μm^{-1})	0.058	0.060	0.025	0.028	0.024	0.024
Normalized surface area of bonds (μm^{-1})	0.114	0.119	0.047	0.052	0.039	0.043

one will use a constant intensity λ with respect to the orientation u. We have:

$$r(h) = K(h)/K(0) = \exp(-\pi\lambda h), \tag{3}$$

$$Q(h) = q^{(2-r(h))} \quad \text{and} \quad Q(l) = q^{1+\pi\lambda h},$$

Only the plaster prepared at 70°C presents a $r(h)$ close to an exponential function. We get the following estimations of λ:

$\lambda = 0.106/\pi = 0.034$ (by linear regression of $\log(r(h))$,

$\lambda = 1/8.5\pi = 0.037$ (by fitting the curve $(r(h),\ 70°G = 100)$.

However, the crystals are not similar to Poisson polyhedra and therefore more realistic shapes must be considered.

4.3.4. Parallelepiped grain

This type of grains was proposed for plaster in a previous study [1]. One considers a rectangular parallelepiped with a square basis (side L_2) and height L_1. For this grain, after a uniform rotation, we get:

$$K(h) = \int_\alpha \int_\beta (L_1 - h\cos\alpha)(L_2 - h\sin\alpha\cos\beta) \times (L_2 - h\sin\alpha\sin\beta)\,\mathrm{d}\alpha\,\mathrm{d}\beta, \tag{4}$$

where each term of the integrand must be positive (otherwise the product is set to zero), and $r(h) = K(h)/K(0)$, with $K(0) = L_1^* L_2^2$.

When $h < L_2$, $K(h)$ has a simple expression [7]

$$K(h) = L_1 L_2^2 - \frac{1}{2}(L_1 L_2 + 2L_2^2)h + \frac{2}{3\pi}(L_1 + 2L_2)h^2 - \frac{h^3}{4\pi}. \tag{5}$$

For larger values of h, we use a numerical computation of $K(h)$. We estimate the two parameters L_1 and L_2, by solving the following system, with $L_1 > L_2 > 0$:

$$L^2 = L_1^2 + 2L_2^2, \quad L_2 < L_1, \quad -4r'(0) = \frac{S}{V} = \frac{2L_2 + 4L_1}{L_1 L_2}. \tag{6}$$

It is derived from the following two properties:

- The correlation length L (for which $r(L) = 0$) is given by the largest diagonal of the grain,
- $-4r'(0)$ is the ratio surface/volume of the grain.

The estimated values of L_1 and L_2 are given in Table 7. Only the plaster prepared at 70°C gives a good fit of $r(h)$, even if it is not so good as the Poisson polyhedra model (Fig. 5). For this material, the estimated lengths are close to the values obtained on micrographs, as seen from the comparison between direct measurements [1] and the result obtained for the fixed parallelepiped in Table 7.

Table 7
Estimation of the parameters of the gypsum grains

	Gypseous	Reference	70°
Direct measurement			
L (μm)	10	25	53.5
l (μm)	1.25	3	9.5
e (μm)	0.75	1.75	5.5
L/l	8.00	8.33	5.63
Fixed parallelepiped			
L_1 (μm)	60.4	50.6	58.2
L_2 (μm)	1.68	4.44	10.2
L_1/L_2 (μm)	35.95	11.40	5.71
Poisson parallelepiped			
L_1 (μm)	75	36	19
L_2 (μm)	2.14	5.33	9.5
L_1/L_2 (μm)	35	6.5	2

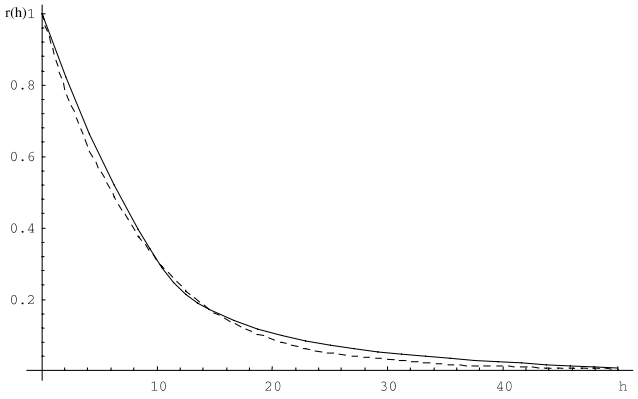

Fig. 5. Comparison between experimental (dashes) and theoretical curves $r(h)$ for the plaster prepared at 70°C ($G = 550$); parallelepiped grain; the distance h is expressed in μm.

4.3.5. Poisson parallelepiped

To account for the real material, where a large range of sizes of needles is observed, we consider now Poisson parallelepipeds with a uniform orientation. They are obtained from nonisotropic Poisson planes given by Poisson points with an intensity made of weights λ_i over three orthogonal directions. It is equivalent to consider parallelepipeds with edges following exponential distributions with parameters λ_i. Here, we will keep two parameters by setting $\lambda_3 = \lambda_2$. The average properties of the grain (volume, surface area, integral of mean curvature M) are given by

$$\overline{V}(A') = \frac{1}{\lambda_1\lambda_2^2},$$
$$\overline{S}(A') = \frac{1}{\lambda_1\lambda_2^2}(4\lambda_2 + 2\lambda_1), \tag{7}$$
$$\overline{M}(A') = \pi\frac{2\lambda_1 + \lambda_2}{\lambda_1\lambda_2.}$$

These can be used to estimate the specific connectivity number of the Boolean model in R^3 from Eq. (A.15).

The normalized covariogram $r(h)$ is

$$r(h) = \frac{4}{\pi^2}\int_0^{\pi/2} \exp(-\lambda_1 h\cos\alpha)\,d\alpha \int_0^{\pi/2} \exp(-\lambda_2 h \times \sin\alpha(\cos\beta + \sin\beta))\,d\beta. \quad (8)$$

It is computed numerically for a set of values of the parameters. We use $1/\lambda_1$ and the ratio $g = \lambda_2/\lambda_1$, which should be of the order of 10 for plaster, as L_1/L_2.

In addition to the plaster prepared at 70°C, the reference material shows a good fit of the curve $r(h)$, except on the beginning of the curve (due to the roughness of the grains) (Fig. 6). However, the gypseous medium gives a poor estimation, since for the magnification $G = 550$ the ratio is of the order of 35 ($\gg$10), which is too high, and $1/\lambda_1$ is close to 75 μm, which is not realistic; for the magnification $G = 1000$, we find $g > 1000$, which cannot be accepted. In fact, this material shows many aggregated needles, with the shape of stars or sea urchins, which could be properly modelled in an extension of the model, by means of appropriate grains.

A comparison between the lengths obtained from the models and from a direct observation is given in Table 7. The reference gives a larger average length than for the plaster prepared at 70°C, as opposed to the direct observation, but the correct decrease of length ratio with temperature is obtained for the two sets of data.

For the Poisson parallelepiped, we get the properties reported in Table 8. We observe an increase of the average volume of grains with temperature, while the intensity decreases; this again illustrates the coarsening of the texture for an almost constant volume fraction. The connectivity number of grains is negative (and correlatively is positive for pores), which is typical of an interconnected matrix of gypsum. This negative values reflects the fact that the genus G_V is larger than the number of gypsum connected components N_V, as a result of the presence of numerous branches in the gypsum skeleton.

We also tried to test a model with three parameters, setting $\lambda_2 \neq \lambda_3$. No significant improvement of fits was obtained, to the expense of one additional unknown, and therefore it is better to limit our approach to the two selected parameters.

Table 8
Main properties of the the Poisson parallelepiped, and of the Boolean model

	Gypseous	Reference	70°C
$V(A')$ (μm^3)	344.4	1104.3	1714.7
$S(A')$(μm^2)	652	858.8	902.5
$M(A')$(μm)	16729	1583	298.5
$Nv(A)$–$Gv(A)$	−2.45	−0.02	−0.00154
teta (μm^{-3})	2.67E − 03	8.10E − 04	4.50E − 04

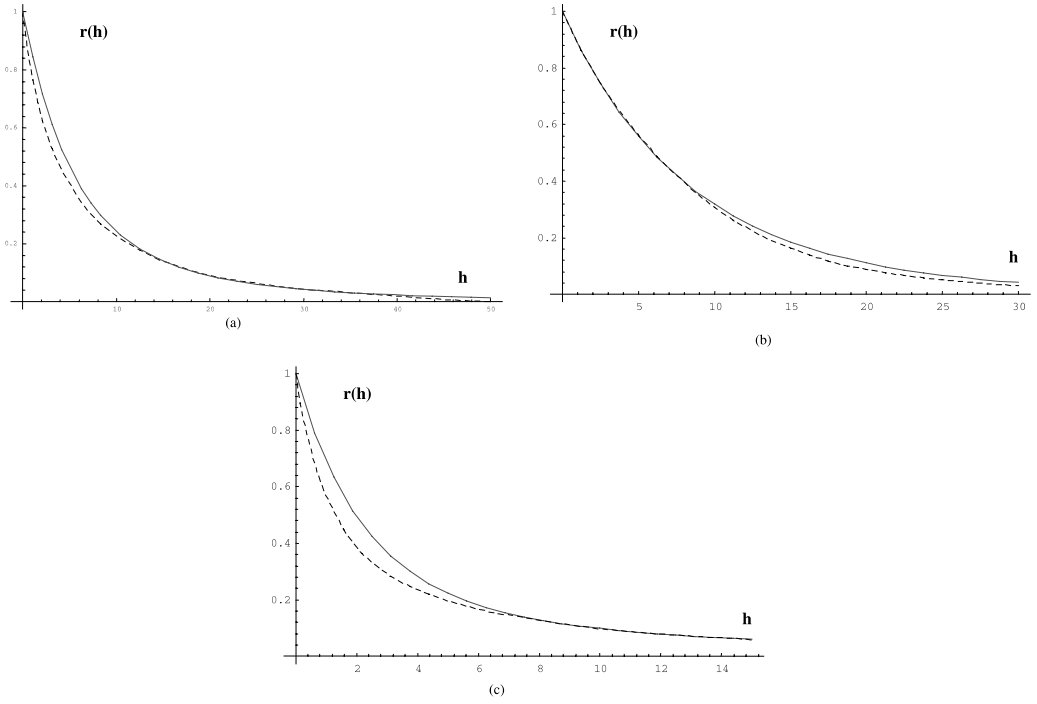

Fig. 6. Comparison between experimental (dashes) and theoretical curves $r(h)$; reference (a); 70°C (b); gypseous (c)); primary grains of the Boolean model: Poisson parallelepiped; the distance h is expressed in μm.

5. Prediction of elastic properties from third-order estimates

5.1. Introduction

In this section, we are interested in the use of probabilistic models, that describe the plaster microstructure, to predict some aspects of the mechanical properties of this porous material [8]. We consider a homogeneous and isotropic gypsum matrix with given elastic properties (compression modulus k and shear modulus μ, obtained from the self-consistent model and assuming an isotropic distribution of orientation of crystallites), and will look for estimates of the macroscopic properties of plaster considered as a porous medium. Its Young's modulus E, known from experimental measurements, can be expressed as:

$$\frac{1}{E}=\frac{1}{3\mu}+\frac{1}{9k}. \tag{9}$$

One will make use of known bounds for μ et k, from which can be derived bounds for E.

5.2. Bounds of first and of second-order

For any two phase medium, a first and simple set of bounds can be obtained from the volume fraction of phases, the Voigt and Reuss bounds expressed as the arithmetic and the harmonic averages (using $\langle\rangle$ for averaging a variable)

$$\begin{aligned}&\langle\mu^{-1}\rangle^{-1}\leqslant\mu^{\hom}\leqslant\langle\mu\rangle,\\&\langle k^{-1}\rangle^{-1}\leqslant k^{\hom}\leqslant\langle k\rangle.\end{aligned} \tag{10}$$

If the geometry of the composite is isotropic, the overall moduli are enclosed in the Hashin and Shtrikman lower (−) and upper bounds [9]

$$\begin{aligned}\mu^{H\pm}&=\left\langle\mu\times\left(1+\frac{\beta^{\pm}(\mu-\mu^{\pm})}{\mu^{\pm}}\right)^{-1}\right\rangle\cdot\left\langle\left(1+\frac{\beta^{\pm}(\mu-\mu^{\pm})}{\mu^{\pm}}\right)^{-1}\right\rangle^{-1},\\k^{H\pm}&=\left\langle k\times\left(1+\frac{\alpha^{\pm}(k-k^{\pm})}{k^{\pm}}\right)^{-1}\right\rangle\cdot\left\langle\left(1+\frac{\alpha^{\pm}(k-k^{\pm})}{k^{\pm}}\right)^{-1}\right\rangle^{-1},\end{aligned} \tag{11}$$

where

$$\alpha^{\pm}=\frac{3k_{\pm}}{3k_{\pm}+4\mu_{\pm}},\quad \beta^{\pm}=\frac{6(k_{\pm}+2\mu_{\pm})}{5(3k_{\pm}+4\mu_{\pm})}$$

and μ^{+} (resp. k^{+}) is the largest value of μ_i (resp. k_i) over the phases (i), and μ^{-} (resp. k^{-}) the lowest value. For porous media, the lower bound is equal to zero, so that the upper bound can be used as an estimate.

5.3. Third-order bounds

Milton [10] made a simplification of the order three bounds given by Beran and Molyneux for k [11], and by Mc Coy for μ [12], in the case of two phases media (like here pores (2) and gypsum (1)) for the compression modulus k and for the shear modulus μ, by using two coefficients ζ_1 and η_1 which depend on the morphology of materials through their three point probability $Q(h_1,\ h_2)$. If $\delta\mu=\mu_1-\mu_2$ and $\delta k=k_1-k_2$, these bounds are equal to the third-order in $\delta\mu$ and δk, when they tend to zero (if phases (1) and (2) have a low mechanical contrast) [10]. For porous media, the lower bounds are given by $k_{-}=\mu_{-}=0$. The third-order upper bounds k_{+} and μ_{+} are given as a function of the solid fraction p (the pore volume fraction being $q=1-p$) by [13]

$$k_{+}=\frac{4p\mu k\zeta_1(p)}{3(1-p)k+4\mu\zeta_1(p)}, \tag{12}$$

$$\mu_{+}=\frac{p\mu}{1+\frac{6(1-p)(k+2\mu)^2}{5\mu(4k+3\mu)\zeta_1(p)+(3k+\mu)^2\eta_1(p)}} \tag{13}$$

The coefficient $\zeta_1(p)$ can be expressed as follows [10]:

$$\text{in 3D},\ \zeta_1(p)=\frac{9}{4pq}\int_0^{+\infty}\frac{\mathrm{d}r}{r}\int_0^{+\infty}\frac{\mathrm{d}s}{s}\int_{-1}^{+1}(3u^2-1)\times P(s,r,\theta)\,\mathrm{d}u \tag{14}$$

$$\text{in 2D},\ \zeta_1(p)=\frac{4}{\pi pq}\int_0^{+\infty}\frac{\mathrm{d}r}{r}\int_0^{+\infty}\frac{\mathrm{d}s}{s}\int_0^{\pi}\cos(2\theta)\times P(s,r,\theta)\,\mathrm{d}u, \tag{15}$$

where $P(s,r,\theta)$ is the probability that the three points $\underline{x},\underline{x}+\underline{s}$ and $\underline{x}+\underline{r}$ are in phase 1 with fraction p (θ is the angle between the vectors $\underline{s}$ and $\underline{r}$ and $u=\cos\theta$).

We have, $0\leqslant\zeta_1\leqslant 1$. Exchanging components (1) and (2), we define ζ_2, such that $\zeta_2=1-\zeta_1$.

The parameter ζ_1 can be computed numerically from the knowledge of $P(s,r,\theta)$, which depends on a given model of random microstructure. For a Boolean model with grains A', it is given by Eq. (A.11). In practice, with a good approximation, $\zeta_1(p)\approx ap+\zeta(0)$ [14,15]. For instance,

In 3D, for spheres, $\zeta_1(p)=0.5615p$ [14,16,17].
In 2D [15,19], for discs, $\zeta_1(p)=2p/3$ [18].
for Poisson polygons, $\zeta_1(p)=0.5057p+0.2274$
for Poisson rectangles (with $\lambda_1=\lambda_2$), $\zeta_1(p)=0.236+0.495p$
for squares, $\zeta_1(p)=0.079+0.601p$.

The coefficients η_1 is defined by

$$\eta_1(p)=\frac{5\zeta_1(p)}{21}+\frac{150}{7pq}\int_0^{+\infty}\frac{\mathrm{d}r}{r}\int_0^{+\infty}\frac{\mathrm{d}s}{s}\times\int_{-1}^{+1}1/8(35u^4-30u^2+3)P(s,r,\theta)\,\mathrm{d}u. \tag{16}$$

Table 9
Comparison of estimations of elastic properties by upper bounds

Upper bounds	k (Gpa)	μ (Gpa)	E (Gpa)
Voigt	17.87	6.24	16.77
Hashin & Shtrikman	7.95	4.15	10.62
Boolean model (sphere)	2.84	2.19	5.23
Experimental data	Nonavailable	Nonavailable	3.70

The parameter η_1 is known for a Boolean model of spheres. With a good approximation, we have [14,18] $\eta_1(p) = 0.711p$.

In a first approach, the two functions $\zeta_1(p)$ and $\eta_1(p)$ corresponding to the Boolean models with random parallelepipeds were not computed. Instead, the upper bound is given for a gypsum solid phase texture made of a Boolean model of spheres (with a single radius). For this calculation, the following estimates of moduli of nonporous gypsum were used: $k = 42.55$ Gpa and $\mu = 14.85$ Gpa. For the porous medium (with a 0.58 pore volume fraction) k and μ are obtained from Eqs. (12) and (13), and the Young's modulus E is deduced from Eq. (9). It is measured on gypsum by a four points bending test. The results are given in Table 9, where the available upper bounds can be compared to experimental data for the reference material; as expected, the upper bound given by the Boolean model gives an estimation higher than the experimental modulus, but this bound is much closer to the experimental measurement than the Voigt and Hashin–Shtrikman bounds, while the self-consistent model would predict null moduli for a pore volume fraction larger than 0.5.

6. Conclusion

The complex geometry of the textures developed in plasters could be described by means of a model of random medium, the Boolean model with parallelepiped grains. This first approach might be improved by the introduction of more realistic shapes like aggregates of needles, for a better description of media with a gypseous texture, at the expense or a more complex modeling. The models were used to estimate some contact properties between overlapping crystals, to be related to the toughness of the material, and to predict the overall elastic properties of plasters from their morphology. Still some efforts must be done in this direction, in order to progress in the prediction of the physical behaviour of plasters from their morphology.

Appendix A. Basic morphological measurements

It can be shown [3,5] that in the n-dimensional space, $n+1$ measurements satisfy to the experimental requirements (invariance by translation, continuity, access over restricted fields of measurement, additivity), the *Minkowski functionals of degree i*: $W_i(\lambda A) = \lambda^i W_i(A)$. We have for $n = 1, 2, 3$:

In R, $W_0(A)$ is the length of the set A and $W_1(A)$ is equal to 2 for a single object (segment).

In R^2, $W_0(A)$ is the area of A, $2W_1(A)$ its perimeter and $2W_2(A)$ is equal to $2\pi N(A)$, where $N(A)$ is the connectivity number (difference between the number of connected components of A and the number of holes that it contains).

In R^3, $W_0(A)$ is the volume of A, $3W_1(A)$ its surface area, $3W_2(A)$ the integral mean curvature $M(A)$. Finally, $3W_3(A)$ is equal to $4\pi(N–G)$, where N is the number of connected components of A, and G its genus (maximal number of closed curves that can be drawn on its boundary ∂A, without disconnecting it (the genus is 0 for a sphere and 1 for a torus)).

Appendix B. Basic morphological transformations

One defines the translated set at point x, K_x and the transposed set $\breve{K}$ by:

$$K_x = \{x + y, y \in K\},$$

$$\breve{K} = \{-x, x \in K\}.$$

A set X is transformed by dilation by K by recording the locations x, where K_x hits X. Similarly, the set A is eroded by K when recording the locations x where K_x remains included in X. Using the Minkowski substraction (noted Θ) and addition (noted $\oplus$), the dilation and the erosion of X by K, noted $X \oplus \breve{K}$ and $X \Theta \breve{K}$ are expressed by:

$$X \oplus \breve{K} = \{x, K_x \cap X \neq \emptyset\}, \tag{A.1}$$

$$X \Theta \breve{K} = \{x, K_x \subset X\}, \tag{A.2}$$

$$X \oplus Y = \cup_{x \in X,\ y \in Y}\{x + y\} = \cup_{x \in X} Y_x = \cup_{y \in Y} X_y$$

with

$$X \Theta Y = \cap_{y \in Y} X_y = (X^c \oplus Y)^c. \tag{A.3}$$

The operations of erosion and of dilation are dual from each other by complementation; i.e., it is equivalent to transform a set (like pores) by erosion or to transform its complementary set (like grains) by dilation.

Appendix C. Characterization of a random set

A random set A is known from its *Choquet's capacity* $T(K)$ [5], defined over the compact sets K. We have:

$$T(K) = P(A \cap K \neq \emptyset) = P(O \in A \oplus \breve{K}) = 1 - P(K \subset A^c) = 1 - Q(A). \quad (A.4)$$

For a stationary random closed set A, $T(K_x) = T(K)$ ($T(K)$ is invariant by translation). If in addition A is ergodic, $T(K)$ can be estimated (we use a * for an estimator) from a single realization (or image) of A by:

$$T(K)^* = P(x \in A \oplus \breve{K})^* = V_V(A \oplus \breve{K})^*. \quad (A.5)$$

Using image analysis measurements, we will consider various compact sets K, each one bringing its own piece of information on A.

If $K = x$, $T(x) = P\{x \in A\} = p$. We obtain the volume fraction p of A ($V_V(A)$).

If $K = \{x, x+h\}$,

$$T(x, x+h) = P(x \in A \cup A_{-h}),$$
$$Q(x, x+h) = P(x \in A^c \cap A^c_{-h}), \quad (A.6)$$

where $Q(x, x+h) = Q(h)$ is the covariance of A^c.

If K is the segment with the length l, $Q(l)$ is the probability for a segment l to be included in A^c, obtained by linear erosion of A^c.

If K is the hexagon with diameter d, then $Q(d)$ is obtained by hexagonal erosion of A^c.

Appendix D. Main properties of the Poisson point process and of the Boolean model

D.1. Poisson point process

The uniform Poisson point process with intensity θ has the following properties: the numbers of points $N(K_i)$ in the compact sets K_i are independent random variables when the K_i have no intersection. Moreover, $N(K)$ is a Poisson random variable with parameter $\theta\mu(K)$, where $\mu(K)$ is the Lebesgue's measure (volume in n-dimensional space) of K. Therefore,

$$P_n(K) = P(N(K) = n) = \frac{(\theta\mu(K))^n}{n!} \exp(-\theta\mu(K)) \quad (A.7)$$

and

$$T(K) = 1 - \exp(-\theta\mu(K)). \quad (A.8)$$

D.2. Properties of the Boolean model [3–7]

The Choquet's capacity is deduced from the fact that the average number of primary grains hit by K follows a Poisson distribution with the intensity $\theta\overline{\mu}(A' \oplus \breve{K})$

$$T(K) = 1 - Q(K) = 1 - \exp(-\theta\overline{\mu}(A' \oplus \breve{K})) = 1 - q^{\overline{\mu}(A' \oplus \breve{K})/\overline{\mu}(A')} \quad \text{with } q = P\{x \in A^c\}, \quad (A.9)$$

From Eq. (A.9) can be deduced:

– the *covariance* of the complementary set of grains A_c, $Q(h)$

$$Q(h) = P\{x \in A^c, x+h \in A^c\} = q^2 \exp(\theta K(h)) = q^{2-r(h)}, \quad (A.10)$$

where $K(h)$ is the *geometrical covariogram* $K(h) = \overline{\mu}(A' \cap A'_{-h})$ (Fig. 7) and $r(h)$ is the reduced geometrical covariogram $r(h) = K(h)/K(0)$.

– the *three points probability* for A^c

$$Q(h_1, h_2) = P\{x \in A^c, x+h_1 \in A^c, x+h_2 \in A^c\} = \exp\left(-\theta\overline{\mu}_n\left(A' \cup A'_{-h_1} \cup A'_{-h_2}\right)\right) = q^{3-r(h_1)-r(h_2)-r(h_2-h_1)+s(h_1,h_2)} \quad (A.11)$$

with

$$s(h_1, h_2) = \frac{\overline{\mu}_n\left(A' \cap A'_{-h_1} \cap A'_{-h_2}\right)}{K(0)}. \quad (A.12)$$

In the case of convex primary grains, one can use the Steiner's formula: $\overline{\mu_n}(A' \oplus \lambda\breve{K})$ is a polynomial of degree k in λ, where K is a compact convex set in Rk. Its coefficients depend on the expectation of the Minkowski functionals of A'. From dilation by convex structuring elements, we can estimate

$$E\{W_i(A \oplus \breve{K})\} = \sum_{k=0}^{n-1} \binom{n-1}{k} W_{k+i}(A) W_{n-k}(A), \quad (A.13)$$

where $E\{W_i(A \oplus \breve{K})\}$ is the average value of $W_i(A \oplus \breve{K})$ over all the rotations of K. For a segment of length l, $Q(l)$ is expressed as

$$Q(\ell) = \exp(-\theta\overline{\mu_n}(A' \oplus \ell)) = \exp(-\theta(K(0) - \ell K'(0)) = q^{1-\ell r'(0)}). \quad (A.14)$$

For this model, the curve $Q(\ell)$ is a decreasing exponential function of ℓ, which can be used to test the model.

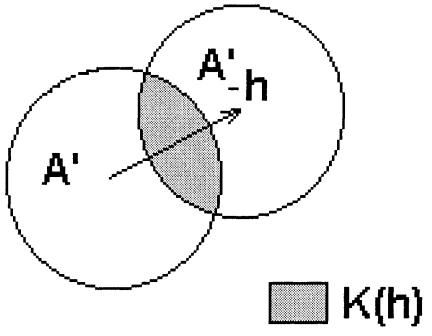

Fig. 7. Definition of the geometrical covariogram (area of the shaded zone for a planar object).

The specific connectivity number of the Boolean model in R^3 was derived by Miles, as a function of the average properties of the convex grain [3]

$$N_V(A) - G_V(A) = q\left[\theta - \frac{\theta^2\overline{M}(A')\overline{S}(A')}{4\pi} + \frac{\pi}{6}\left(\frac{\theta\overline{S}(A')}{4}\right)^3\right]. \tag{A.15}$$

References

[1] Dany C, Reynaud P, Fantozzi G, Amathieu L, Caspar JP. Influence de la microstructure du plâtre sur ses propriétés mécaniques. Eurogypsum 1996:32.

[2] Kolher R. A segmentation system based on thresholding. Comp Graphics and Image Proc 1981;15:319–38.

[3] Serra J. Image analysis and mathematical morphology. New York: Academic Press; 1982.

[4] Matheron G. Eléments pour une théorie des milieux poreux. Paris, 1967.

[5] Matheron G. Random sets and integral geometry. New York: Wiley; 1975.

[6] Matheron G. Ensembles fermés aléatoires, ensembles semi-markoviens et polyédres poissoniens. Advances in applied probability IV 1972;3:508–41.

[7] Greco A, Jeulin D, Serra J. The use of texture analyser to study sinter structure: application to the morphology of calcium ferrites encountered in basic sinters of rich iron ores. J Microscopy 1979;116:199–211.

[8] Jeulin D. Probabilistic models of structures PROBAMAT- 21 century: probabilities and materials. In: G.N. Frantziskonis, editors. 1998; p. 233–257.

[9] Hashin Z, Shtrikman S. A variational approach to the theory of the elastic behaviour of multiphase materials. J Mech Phys Solids 1963;11:127–40.

[10] Milton GW. Bounds on the elastic and transport properties of two-component composites. J Mech Phys Solids 1982;30:177–91.

[11] Beran MJ, Molyneux J. Use of classical variational principles to determine bounds for the effective bulk modulus in heterogeneous media. Q Appl Math 1966;24:107–18.

[12] Mc Coy JJ. On the deplacement field in an elastic medium with random variations of material properties. Recent Adv Eng Sci, Ed Gordon and Breach (NY) 1970;5:235–54.

[13] Berryman JG, Milton GW. Microgeometry of random composites and porous media. J Phys D: Appl Phys 1988;21:87–94.

[14] Berryman JG. Variational bounds on elastic constants for the penetrable sphere model. J Phys D: Appl Phys 1985;18:585–97.

[15] Jeulin D, Le Coënt. Morphological modeling or random composites. Proc of CMDS8 Int Symposium, June 1995, Varna Bulgaria, In: Markov KZ, editor. Singapore: World Scientific Publishing Company; 1996. p. 199–206.

[16] Torquato S, Stell G. J Chem Phys 1983;79:1505.

[17] Torquato S, Lado F. Effective properties of two phase disordered composite media: II evaluation of bounds on the conductivity and bulk modulus of dispersions of impenetrable spheres. Phys Rev B 1986;33:6428.

[18] Torquato S. Random heterogeneous media: microstructure and improved bounds on effective properties. Appl Mech Rev 1991;44:37–76.

[19] Le Coënt, Jeulin D. Bounds of effective physical properties for random polygon composites. Paris: CR Acad Sci 1996; 323 (série IIb):299–306.